Journal of Physics: Condensed Matter

PAPER • **OPEN ACCESS**

Impedance response of electrochemical interfaces: part II-chemisorption

To cite this article: Jun Huang and Chen-Kun Li 2021 *J. Phys.: Condens. Matter* **33** 164003

OPEN ACCESS
IOP Publishing
Journal of Physics: Condensed Matter
J. Phys.: Condens. Matter **33** (2021) 164003 (11pp)
https://doi.org/10.1088/1361-648X/abef9d

Impedance response of electrochemical interfaces: part II-chemisorption

Jun Huang[1,3,*] **and Chen-Kun Li**[2]

[1] Institute of Energy and Climate Research, Theory and Computation of Energy Materials (IEK-13), Forschungszentrum Juülich GmbH, 52425 Juülich, Germany
[2] College of Chemistry and Chemical Engineering, Central South University, 410083 Changsha, People's Republic of China

E-mail: j.huang@fz-juelich.de

Received 16 January 2021, revised 26 February 2021
Accepted for publication 17 March 2021
Published 20 April 2021

Abstract

Physical modeling helps to acquire fundamental insights from experimental data when electrochemical impedance spectroscopy is employed for mechanistic understandings of electrocatalytic reactions. Herein, we report an analytical model for chemisorption impedance with a consistent treatment of ion transport in the solution and electron transfer on the electrode surface. Our formulation avoids both *a priori* decoupling of double-layer charging and electron transfer reaction, and a strict separation of double-layer charging and ion transport. Ion transport in the entire solution region is described by the Poisson–Nernst–Planck theory and electron transfer kinetics on the electrode surface by the Frumkin–Butler–Volmer theory. Surface dipoles caused by partially charged chemisorbates are considered. The classical Frumkin–Melik–Gaikazyan model for chemisorption is retrieved as a limiting case. The obtained formula is validated using experimental data of hydrogen adsorption at Pt(111). Characteristic frequencies and asymptotic behaviors of chemisorption impedance are analyzed.

Keywords: electrocatalytic interface, electric double layer, electrochemical impedance, Ershler–Dolin model, partial charge transfer

Supplementary material for this article is available online

(Some figures may appear in colour only in the online journal)

1. Introduction

Electrocatalysis provides us with fundamental knowledge and promising technologies, such as fuel cells and water electrolysers, to meet the grand challenge of securing sustainable and clean energy. All electrocatalytic reactions have an elementary process in common, viz, chemisorption, which refers to the chemical binding of a molecule or an ion from the electrolyte solution onto the electrode surface, as shown in figure 1(a) [1–3]. Chemisorption occurs in the electrochemical double layer (EDL), a complicated nanoscale interfacial region with significant distributions of electric potential and ion concentration [4, 5]. On one hand, chemisorption kinetics is influenced by the local reaction condition in the EDL [6–9]. For instance, employing a cluster model with point charges placed above and below the cluster surface, Pacchioni and Bagus showed that electrostatic interactions between point charges and a chemisorbed CO significantly shift the vibrational frequency of the CO chemisorbed on transition-metal surfaces [10]. In addition, an experimental study of Climent, García-

[3] Present address: Institute of Theoretical Chemistry, Ulm University, 89069 Ulm Germany.
[*] Author to whom any correspondence should be addressed.

Araez, and Feliu showed that the identity of alkali cations affects the vibrational frequency of (bi)sulphates chemisorbed on Pt(111) electrodes via regulating the local electric field [11]. On the other hand, chemisorption changes the EDL, in turn, by forming partially charged chemisorbates on the electrode surface. As for the latter aspect, recent works have revealed that chemisorption can lead to nonmonotonic surface charging behavior of the EDL [7, 12–14].

Obtaining fundamental parameters of chemisorption is crucial for mechanistic understanding of electrocatalytic reactions and the subsequent rational design of more active electrocatalysts [15, 16]. A principal method for this purpose is electrochemical impedance spectroscopy (EIS) [17–20]. The difficulty lies in separating individual contributions from the partial electron transfer process, the EDL charging process, and the mass transport process in the electrolyte solution. Reliable acquisition of physical parameters from the EIS data requires a physical model; the prevailing one for chemisorption being the Frumkin–Melik–Gaikazyan model, which is an extension of the Ershler–Dolin model by including a Warburg element to describe diffusion of the adsorbing species [17–22].

The electrical circuit representation of the Frumkin–Melik–Gaikazyan model is depicted in figure 1(b). In addition to the solution resistance R_s, the model consists of a double-layer capacitance C_{dl} and a reaction branch ($R_{ad} - C_{ad} - W$) in parallel connection. The reaction branch includes a charge-transfer resistance R_{ad}, a pseudo-capacitance of chemisorption C_{ad}, and a diffusion impedance W. A frequency-dependent capacitance can be derived from the Frumkin–Melik–Gaikazyan model

$$C(\omega) = \frac{1}{j\omega(Z - R_s)} = C_{dl} + \frac{C_{ad}}{j\omega C_{ad}(R_{ad} + W) + 1}, \quad (1)$$

where Z is the total interfacial impedance, ω the angular frequency, and W the diffusion impedance, which is often described by the Warburg formula, $W = \sigma_D(j\omega)^{-0.5}$ with σ_D being a coefficient as a function of the diffusion coefficient [23]. $C(\omega)$ is asymptotic to C_{dl} when $\omega \to \infty$, and to $C_{dl} + C_{ad}$ when $\omega \to 0$. In the intermediate frequency range, $C(\omega)$ is manifested as an arc which becomes more squashed as the diffusion impedance is more significant [20, 22, 24]. Walters *et al* extended the Frumkin–Melik–Gaikazyan model to consider partial charge transfer [25].

The Frumkin–Melik–Gaikazyan model and the existing extensions have certain limitations. Firstly, it is assumed *a priori* that the EDL charging process and the electron transfer process are decoupled. Consequently, the corresponding electrical circuit elements can be connected in parallel in figure 1(b). Secondly, the EDL charging process and the mass transport process, both belonging to ion transport in the electrolyte solution, are strictly separated and placed in different branches in the circuit. Thirdly, the EDL capacitance is taken as a frequency-independent constant, which is, in the strict sense, problematic as the EDL charging is essentially an ion transport process which shall manifest frequency dispersion [22, 26]. Fourthly, the ion transport process is described using the Warburg formula which has well-defined restrictions [27].

In this paper, we present an analytical model for chemisorption impedance that removes above assumptions. The Frumkin–Melik–Gaikazyan model is retrieved from the new model as a limiting case. The analytical model is first subject to analysis of the asymptotic behavior, then validated (more precisely, compared) with experimental data, and finally used as a transparent tool to analyze characteristic frequencies of the chemisorption impedance. In particular, we explain why the diffusion signature, a 45° line, is absent in previous experimental studies [16, 20] and reveal under what conditions it manifests in the low frequency range.

This paper is a part of a series of theoretical works focused on analytical modeling of the impedance response of electrochemical interfaces [24, 28] and porous electrodes [29–33]. In reference [24] which is of closest relevance to the present work, we have derived an analytical expression for the impedance response of an ideally polarizable electrode. A remarkable finding there is that the series connection of the Helmholtz capacitance and a diffuse-layer part, inherited from the classical Gouy–Chapman–Stern model, tacitly stipulates a zero potential gradient in the solution bulk, which is invalid in rigorous sense. The mathematical techniques involved in the present work are similar to those in reference [24]. Therefore, a detailed derivation of the present work is provided in the supporting information (https://stacks.iop.org/JPCM/33/164003/mmedia) (SI).

2. Theory

We treat a one-dimensional EDL with chemisorption of ions occurring on the electrode surface, figure 1(a). Microscopic models of the chemisorption process, considering electronic and electrostatic interactions and solvent reorganization, have been developed using the model Hamiltonian approach [8, 9, 34, 35]. Such microscopic models are beyond the scope of this work; instead, we use the phenomenological Butler–Volmer theory augmented with the Frumkin correction to describe the electron transfer kinetics of the chemisorption process [36, 37].

The electrolyte solution is restricted to be dilute (<0.1 M); cations and anions are monovalent and have the same diffusion coefficient D. The electrode surface charge is restricted to be small (<0.1 C m^{-2}). Under such circumstance, the Poisson–Nernst–Planck (PNP) theory is valid to describe ion transport in solution [38, 39]

$$\frac{\partial C_+}{\partial \tau} = \frac{\partial}{\partial X}\left(\frac{\partial C_+}{\partial X} + C_+\frac{\partial U}{\partial X}\right), \quad (2)$$

$$\frac{\partial C_-}{\partial \tau} = \frac{\partial}{\partial X}\left(\frac{\partial C_-}{\partial X} - C_-\frac{\partial U}{\partial X}\right), \quad (3)$$

$$0 = \frac{\partial^2 U}{\partial X^2} + \frac{1}{2}(C_+ - C_-), \quad (4)$$

where C_+ and C_- are dimensionless concentrations of cations and anions normalized with respect to the bulk electrolyte concentration c_0, τ is the dimensionless time referenced to λ_D^2/D and X the dimensionless spatial coordinate normalized with respect to the Debye length, $\lambda_D = \sqrt{\epsilon RT/(2F^2c_0)}$, with ϵ being the dielectric permittivity of the bulk solution.

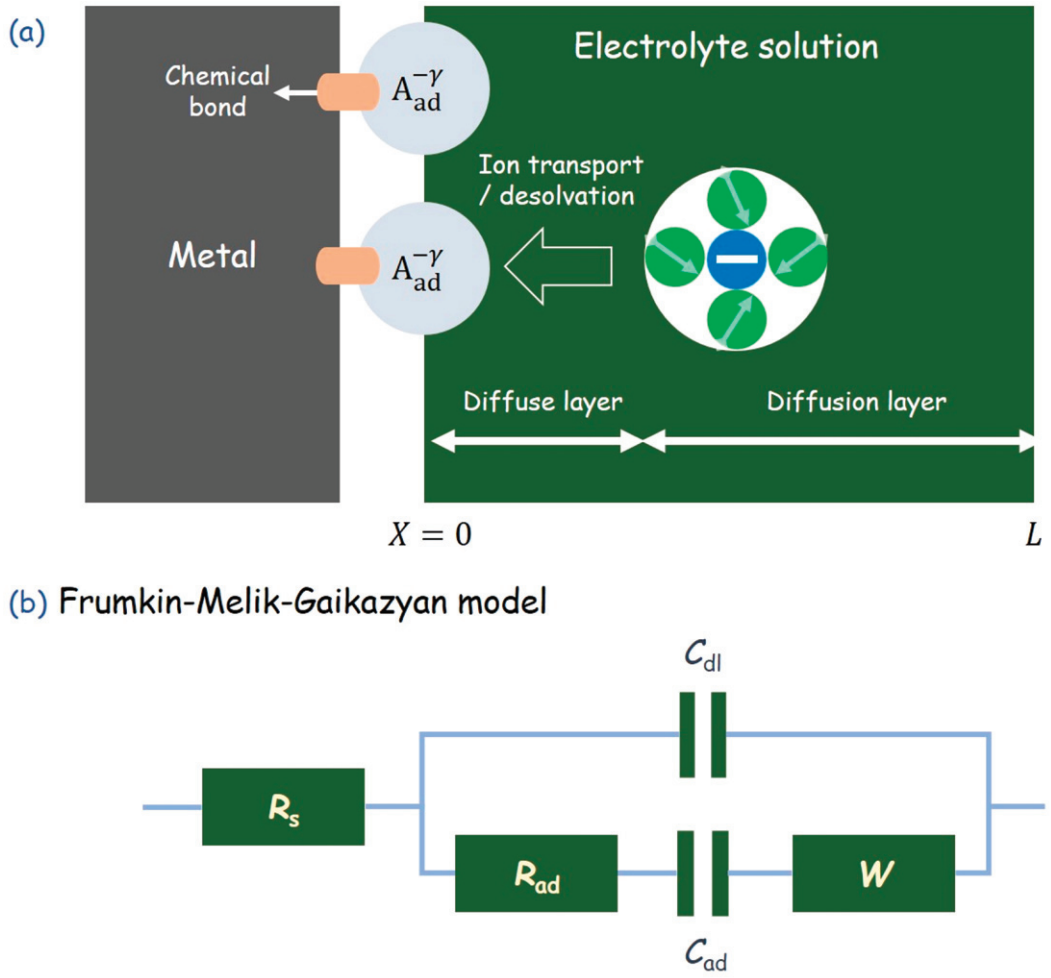

Figure 1. (a) Schematic illustration of the EDL with chemisorption. Note that the boundary between the diffusion layer and the diffuse layer is not strict in real situations. (b) Electrical circuit representation of the Frumkin–Melik–Gaikazyan model. R_s is the resistance of the bulk solution, C_{dl} the double-layer capacitance, C_{ad} the pseudo-capacitance of chemisorption, R_{ad} the charge-transfer resistance of chemisorption, W the diffusion impedance.

The PNP theory is closed with boundary conditions as follows. At the adsorbate plane (AP), $X = 0$, the chemisorption process of anions A^- takes place

$$A^- + {}^* \leftrightarrow A_{ad}^{-\gamma} + (1-\gamma)\,e, \tag{5}$$

where $*$ denotes the adsorption site and γ the remaining electron number on the adsorbate, which has been shown to be dependent on the coverage [40]. The specific adsorption of cations can be treated in the same manner, thus only the final result will be given. According to the Frumkin–Butler–Volmer theory [36, 41], the reaction rate (mol $m^{-2}s^{-1}$), positive-defined for the oxidation direction, is written as

$$J_{ad} = \frac{N_{site}}{N_A}\frac{d\theta}{dt} = k_0\left[C_{-,AP}\,(1-\theta)\exp\left(\frac{\alpha F\eta}{RT}\right) - \theta\,\exp\left(-\frac{(1-\alpha)\,F\eta}{RT}\right)\right], \tag{6}$$

where N_{site} is the number density of adsorption sites, k_0 the rate constant, $C_{-,AP}$ the dimensionless concentration of A^- at the reaction plane which is designated as the AP, θ the coverage of adsorbates, α the effective charge transfer coefficient, and η the overpotential

$$\eta = (1-\gamma)\,(\phi_M - \phi_{AP}) - E_0 - \frac{\xi}{F}\theta, \tag{7}$$

where ϕ_M is the electrode electric potential, ϕ_{AP} the electric potential at the AP, E_0 the standard equilibrium potential of the reaction, and ξ the lateral interaction coefficient. Note that combination of equation (6) and (7) under the static condition leads to the Frumkin adsorption isotherm [42, 43],

$$-\frac{RT}{F}\ln\left(\frac{\theta_s}{1-\theta_s}\right) + (1-\gamma)\,\phi_M + \gamma\phi_{AP,s} - \frac{\xi}{F}\theta_s - E_0 = 0. \tag{8}$$

with the subscript 's' denoting the static condition.

At the AP, the cation flux is zero, namely

$$\frac{\partial C_+}{\partial X} + C_+\frac{\partial U}{\partial X} = 0, \tag{9}$$

and the anion flux is given by

$$\frac{\partial C_-}{\partial X} - C_- \frac{\partial U}{\partial X} = \frac{\lambda_D J_{ad}}{D c_0}. \tag{10}$$

Partially charged adsorbates are assumed to rigidly line up at the AP, forming a surface dipole moment [12, 13], given by

$$\mu_A = -N_{site}\theta e \gamma \delta, \tag{11}$$

where δ is the thickness of the space between the electrode and the AP.

As there is no space charge, the electric potential distribution is linear in the space between the electrode and the AP. Consequently, the dimensionless electric potential at the AP, U_{AP}, is given by

$$U_{AP} = U_M + \frac{\epsilon \delta}{\epsilon' \lambda_D}\frac{\partial U}{\partial X} + \frac{F \mu_A}{\varepsilon' RT}, \tag{12}$$

where U_M the dimensionless electrode electric potential, and ε' the dielectric permittivity of the space between the electrode and the AP. Equation (12) indicates that chemisorption-induced surface dipoles introduce an extra potential change in the space between the electrode and the AP, in addition to the one caused by the net charge stored in the EDL.

In the bulk solution, $X = L = l/\lambda_D$ with l being the thickness of the Nernst diffusion layer, we have $C_+ = C_- = 1$ and the electric potential is taken as the reference, $U = 0$.

Under the static condition, we can obtain $\phi_{AP,s} = \frac{2RT}{F}\operatorname{arcsinh}\left(\frac{F\lambda_D \sigma_M}{2RT\varepsilon}\right)$ from equations (2) and (4), which is the classical result of the Gouy–Chapman model. The surface charge density σ_M is found from

$$\frac{2RT}{F}\operatorname{arcsinh}\left(\frac{F\lambda_D\sigma_M}{2RT\varepsilon}\right) + \sigma_M\left(\frac{\delta}{\varepsilon'}\right) = \left(\phi_M - \phi_{pzc}\right) + \frac{\mu_A}{\varepsilon'}. \tag{13}$$

A detailed derivation of the static conditions described by equations (8) and (13) is provided in the SI. Note that the electric potentials ϕ_M, ϕ_{pzc} (potential of zero charge, pzc) and E_0 are referred to the reversible hydrogen electrode (RHE) scale.

For the sake of obtaining an exact analytical formula, we neglect for the moment static distributions of ion concentration and electric potential. This assumption is rigorously valid only at the pzc, but represents a good approximation in the potential region near the pzc [24]. This assumption was also made in previous theoretical studies from the Macdonald group [44, 45], the Barbero group [46–48], and the Zola group [49], where the impedance response of the PNP theory was obtained in analytical forms, and also in the powerful transmission line model developed by Gaberščček and Moškon [50, 51]. These literature works did not consider the compact Stern layer, nor did they consider the chemisorption reaction on the electrode surface.

The dynamics of the PNP theory in response to a small potential perturbation applied onto the electrode can be solved using the Laplace transform technique, as detailed in the supporting information. After obtaining the perturbed $\tilde{C}_+$ and $\tilde{C}_-$ (overtildes denoting perturbed small quantities), we can solve the total current density $\tilde{i}_{total}$ in response to the potential perturbation. $\tilde{i}_{total}$ is the sum of an EDL charging part $\tilde{i}_{dl}$ and an adsorption reaction part $\tilde{i}_{ad}$,

$$\tilde{i}_{total} = \tilde{i}_{dl} + \tilde{i}_{ad}. \tag{14}$$

$\tilde{i}_{dl}$ is equal to the change rate of the ionic charge density stored in solution, which, via the Laplace transform (namely, replacing $\frac{\partial}{\partial t}$ with $j\omega$), is given by

$$\tilde{i}_{dl} = -j\omega\int_0^L Fc_0\left(\tilde{C}_+ - \tilde{C}_-\right)\lambda_D dX. \tag{15}$$

Using $\frac{FDc_0}{\lambda_D}$ as the reference current density, the dimensionless form of $\tilde{i}_{dl}$, denoted $\tilde{i}_{dl}^{nd}$ (the superscript 'nd' denoting dimensionless quantities), is now written as

$$\tilde{i}_{dl}^{nd} = -j\omega^{nd}\int_0^L \left(\tilde{C}_+ - \tilde{C}_-\right) dX, \tag{16}$$

where ω^{nd} is the dimensionless frequency, $\omega^{nd} = \frac{\omega\lambda_D^2}{D}$.

The adsorption reaction current density is related to the change rate of the adsorbate coverage ($\frac{\partial\theta}{\partial t}$), which is expressed in equation (6). Applying the Laplace transform (namely, replacing $\frac{\partial}{\partial t}$ with $j\omega$) and normalization with respect to the reference current density $\frac{FDc_0}{\lambda_D}$, $\tilde{i}_{ad}$ reads

$$\tilde{i}_{ad}^{nd} = j\omega^{nd}\frac{(1-\gamma)}{\lambda_D c_0}\frac{N_{site}}{N_A}\tilde{\theta} \tag{17}$$

where $(1-\gamma)$ is due to the partial charge transfer. $\tilde{\theta}$ can be expressed as a function of the electrode potential and local reaction conditions, see equation (S45) in the SI.

The dimensionless chemisorption impedance is defined as

$$Z^{nd} = \frac{\tilde{U}_M}{\tilde{i}_{total}}, \tag{18}$$

where $\tilde{U}_M$ represents the dimensionless potential perturbation applied onto the electrode. As the voltage is referenced to $\frac{RT}{F}$ and the current density $\frac{FDc_0}{\lambda_D}$, we know that the reference value for impedance is $\frac{2\lambda_D^2}{C_{GC}^0 D}$. With a step-by-step derivation provided in the SI, we obtain an exact analytical formula for Z^{nd}

$$Z^{nd} = \frac{1}{2}\frac{r_c + L + \frac{1}{j\omega^{nd}}\left(r_c + \frac{\tanh\left(L\sqrt{j\omega^{nd}+1}\right)}{\sqrt{j\omega^{nd}+1}} + \frac{C_{ad}^{nd}\Delta_1}{1+j\omega^{nd}R_{ad}^{nd}C_{ad}^{nd}}\right)}{1 - \operatorname{sech}\left(L\sqrt{j\omega^{nd}+1}\right) + \frac{C_{ad}^{nd}\Delta_2}{1+j\omega^{nd}R_{ad}^{nd}C_{ad}^{nd}}}, \tag{19}$$

where $r_c = \frac{\varepsilon\delta}{\varepsilon'\lambda_D}$ is the ratio between $C_{GC}^0 = \frac{\varepsilon}{\lambda_D}$ representing the Gouy–Chapman capacitance at the pzc and the Helmholtz capacitance ($C_H = \frac{\varepsilon'}{\delta}$), $R_{ad}^{nd} = \frac{2Dc_0}{k_0\theta_s\lambda_D}e^{(1-\alpha)H_s}$ is the dimensionless adsorption resistance with θ_s being the adsorbate coverage at steady state, and $H_s = \frac{F\eta_s}{RT}$ the dimensionless overpotential at steady state, $C_{ad}^{nd} = \frac{2N_{site}}{c_0 N_A \lambda_D}\left(\frac{1}{\theta_s(1-\theta_s)} + \frac{\xi}{RT}\right)^{-1}$ is the dimensionless adsorption capacitance. Δ_1 and Δ_2 are two coefficients taking into account partial charge transfer, and the coupling between electron transfer at the AP and ion transport in the electrolyte solution, given by

$$\Delta_1 = L^2\left[\left((1-\gamma)\,j\omega^{\rm nd}+\sqrt{j\omega^{\rm nd}}\frac{\tanh\left(L\sqrt{j\omega^{\rm nd}}\right)}{L}\right)\right.$$
$$\times\left(\frac{\tanh\left(L\sqrt{j\omega^{\rm nd}+1}\right)}{L\sqrt{j\omega^{\rm nd}+1}}+j\omega^{\rm nd}+\frac{r_{\rm c}}{L}\left(j\omega^{\rm nd}+1\right)\right)$$
$$+\left(j\omega^{\rm nd}+\frac{r_{\rm c}}{L}\left(j\omega^{\rm nd}+\gamma\right)\right)\left(\left(j\omega^{\rm nd}+\gamma\right)\right.$$
$$\left.\left.\times\frac{\tanh\left(L\sqrt{j\omega^{\rm nd}+1}\right)}{L\sqrt{j\omega^{\rm nd}+1}}-(1-\gamma)\,j\omega^{\rm nd}\right)\right],$$

$$\Delta_2 = (1-\gamma)\left(j\omega^{\rm nd}+1\right)\left(\frac{\tanh\left(L\sqrt{j\omega^{\rm nd}+1}\right)}{\sqrt{j\omega^{\rm nd}+1}}\right.$$
$$\left.+(1-\gamma)\,r_{\rm c}\right)-\left(1-\operatorname{sech}\left(L\sqrt{j\omega^{\rm nd}+1}\right)\right)$$
$$\times\left(r_{\rm c}(1-\gamma)\left(j\omega^{\rm nd}+\gamma\right)-\sqrt{j\omega^{\rm nd}}\tanh\left(L\sqrt{j\omega^{\rm nd}}\right)\right).$$

For a given set of experimental conditions, including the electrode potential and electrolytic solution properties, we first solve for the static conditions from equations (8) and (13), and then calculate the impedance response using equation (19).

3. Asymptotic behaviors

The greatest advantage of the analytical formula in equation (19) is that it can be used as a transparent tool to understand the complicated couplings between the EDL charging process, the chemisorption process, and the ion transport process. To this end, asymptotic analysis is a powerful method.

In the high frequency regime, $\omega^{\rm nd}\to\infty$, we have $\Delta_1\sim 2\,(L+r_{\rm c})\left(j\omega^{\rm nd}\right)^{1.5}$, $\Delta_2\sim -j\omega^{\rm nd}\gamma r_{\rm c}\,(1-\gamma r_{\rm c})$, and

$$R_{\rm s}^{\rm nd}=Z^{\rm nd}\left(\omega^{\rm nd}\to\infty\right)=\frac{r_{\rm c}+L}{2-\frac{\gamma r_{\rm c}(1-\gamma r_{\rm c})}{R_{\rm ad}^{\rm nd}}}. \tag{20}$$

which corresponds to the solution resistance $R_{\rm s}$ in the Frumkin–Melik–Gaikazyan model. In the low frequency regime, we have $\omega^{\rm nd}\to 0$, $\Delta_1\sim\gamma^2 r_{\rm c}\tanh(L)$, $\Delta_2\sim(1-\gamma)\,(\tanh(L)+r_{\rm c}\,(1-2\gamma+\gamma\operatorname{sech}(L)))$, and

$$Z^{\rm nd}\left(\omega^{\rm nd}\to 0\right)=\frac{1}{2\,j\omega^{\rm nd}}\frac{r_{\rm c}+\tanh(L)+\gamma^2 r_{\rm c}C_{\rm ad}^{\rm nd}\tanh(L)}{1-\operatorname{sech}(L)+(1-\gamma)\,(\tanh(L)+r_{\rm c}\,(1-2\gamma+\gamma\operatorname{sech}(L)))\,C_{\rm ad}^{\rm nd}}. \tag{21}$$

When $L\gg 1$, $Z^{\rm nd}\left(\omega^{\rm nd}\to 0\right)$ is further simplified to

$$Z^{\rm nd}\left(\omega^{\rm nd}\to 0, L\gg 1\right)=\frac{1}{2\,j\omega^{\rm nd}}\frac{r_{\rm c}+1+\gamma^2 r_{\rm c}C_{\rm ad}^{\rm nd}}{1+(1-\gamma)\,(1+r_{\rm c}-2r_{\rm c}\gamma)\,C_{\rm ad}^{\rm nd}}. \tag{22}$$

In the ideal case of an one-electron transfer reaction, $\gamma=0$, we obtain

$$Z^{\rm nd}\left(\omega^{\rm nd}\to 0, L\gg 1, \gamma=0\right)=\frac{1}{2\,j\omega^{\rm nd}\left(C_{\rm dl}^{\rm nd}+C_{\rm ad}^{\rm nd}\right)}, \tag{23}$$

which agrees with the low-frequency behavior of the classical Frumkin–Melik–Gaikazyan model with $C_{\rm dl}^{\rm nd}=\frac{1}{r_{\rm c}+1}$ being the dimensionless double-layer capacitance normalized with respect to $C_{\rm GC}^0$. The cautious reader shall not worry the factor of 2 in the denominator of equation (23), which disappears if we go back to dimensional quantities using the reference value for impedance $\frac{2\lambda_{\rm D}^2}{C_{\rm GC}^0 D}$.

Equation (23) indicates that the Frumkin–Melik–Gaikazyan model, a limiting case of equation (19), is re-obtained under three conditions: (1) an ideal one-electron transfer reaction ($\gamma=0$), (2) a sufficiently thick Nernst diffusion layer ($L\gg 1$), and (3) 'low' frequencies ($\omega^{\rm nd}\ll 1$). The second and third conditions are usually met in experiments because the thickness of the Nernst diffusion layer, ~100 μm, is around five orders larger than $\lambda_{\rm D}$ which is ~ 1 nm for a 0.1 M aqueous solution at room temperature, and because the highest frequency point in experiments, ~1MHz, corresponds to $\omega^{\rm nd}\sim 10^{-3}\ll 1$ for the common case with $\lambda_{\rm D}\sim 1$ nm and $D\sim 10^{-9}$ m^2 s^{-1}. On the contrary, the first condition is violated in most cases [6].

In general, the total interfacial capacitance calculated from equation (22) is

$$C_{\rm total}^{\rm nd}\left(\omega^{\rm nd}\to 0, L\gg 1\right)=\frac{1+(1-\gamma)\,(1+r_{\rm c}-2r_{\rm c}\gamma)\,C_{\rm ad}^{\rm nd}}{r_{\rm c}+1+\gamma^2 r_{\rm c}C_{\rm ad}^{\rm nd}}. \tag{24}$$

Subtracting $C_{\rm ad}^{\rm nd}$ from $C_{\rm total}^{\rm nd}$, we obtain $C_{\rm dl}^{\rm nd}$ as

$$C_{\rm dl}^{\rm nd}=C_{\rm total}^{\rm nd}-C_{\rm ad}^{\rm nd}=\frac{1-C_{\rm ad}^{\rm nd}\gamma\left(1+3r_{\rm c}-2r_{\rm c}\gamma+r_{\rm c}\gamma C_{\rm ad}^{\rm nd}\right)}{r_{\rm c}+1+\gamma^2 r_{\rm c}C_{\rm ad}^{\rm nd}}. \tag{25}$$

As $\gamma<1$ and $1+3r_{\rm c}-2r_{\rm c}\gamma>0$, a sufficient condition for the occurrence of negative $C_{\rm dl}^{\rm nd}$ is

$$\gamma>\frac{1}{\sqrt{r_{\rm c}}C_{\rm ad}^{\rm nd}}. \tag{26}$$

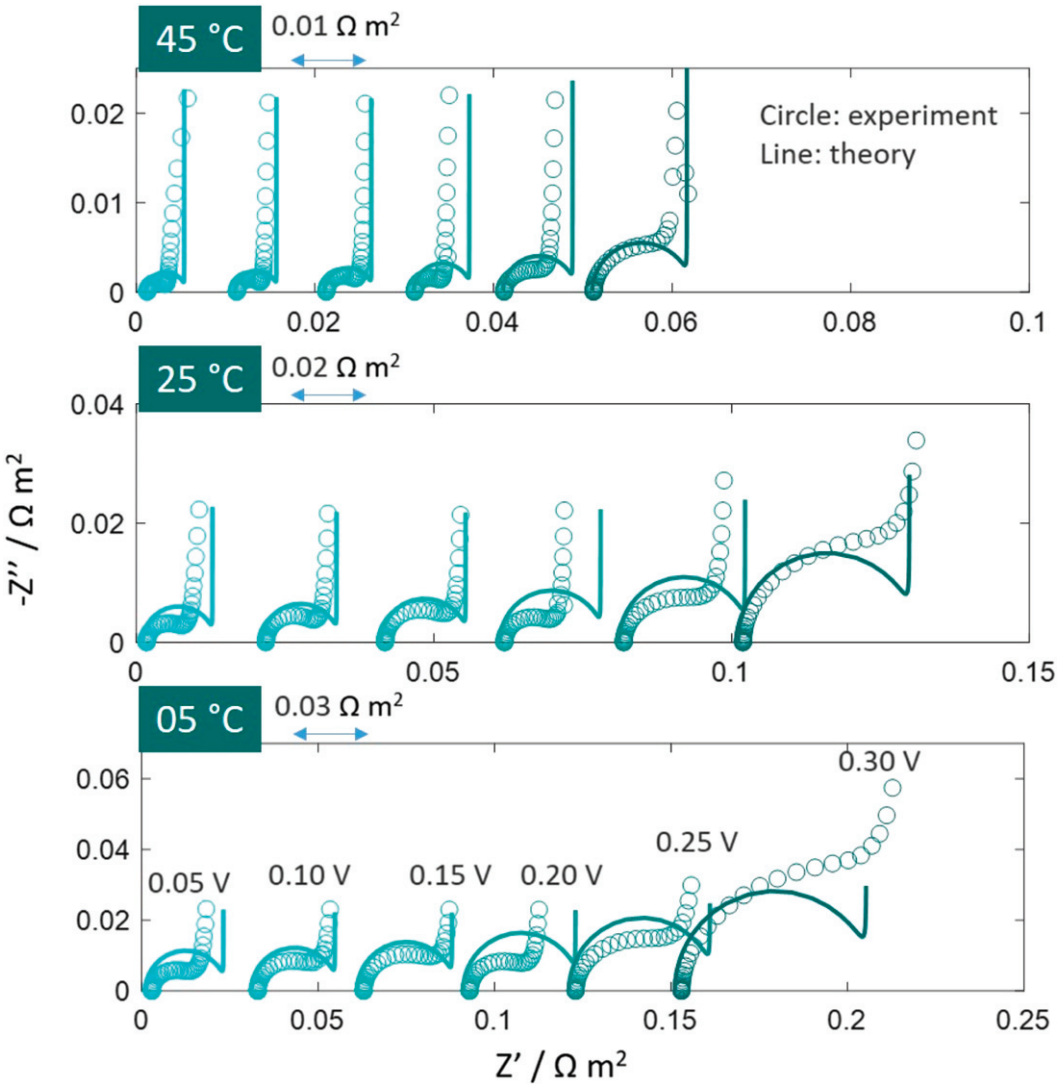

Figure 2. Comparison between the theory (lines) and experimental data (circles) measured for the hydrogen adsorption at Pt(111) in 0.05 M NaOH at three temperatures (5, 25, 45 °C) and six potentials (0.05 V_{RHE} to 0.30 V_{RHE} in a step of 0.05 V) [16]. In each subplot, six EIS curves corresponding to 0.05 V_{RHE} to 0.30 V_{RHE} in a row from left to right are shifted on the real axis by 0.01, 0.02 and 0.03 Ω m^{-2}, respectively. The frequency range is from 10 kHz to 1 Hz with ten points per decade.

The analysis of magnitude shows that $C_{ad}^{nd} \sim 10$ and $r_c \sim 1$ in common experimental conditions. Therefore, the occurrence of negative double-layer capacitance in the presence of chemisorption can be expected when $\gamma > 0.1$, which is a mild condition. In a previous work, we have derived an analytical solution for the double-layer capacitance of the Pt(111)-water interface in the potential range where OH_{ad} occurs [13]. The previous work inherited the framework of the Gouy–Chapman–Stern model and neglected the frequency dispersion of the double-layer capacitance. Nevertheless, we also proposed that chemisorption can lead to negative double-layer capacitance, implying a nonmonotonic surface charging relation, which was first modeled in 2016 [12]. Although it remains a frontier challenge to measure the free charge on the electrode surface and the double-layer capacitance of solid electrodes in presence of chemisorption, a few experiments suggest the occurrence of a nonmonotonic surface charging relation with a second pzc, and therefore, negative double-layer capacitance [7, 14, 52].

4. Comparison with experimental data

We now compare the theoretical formula in equation (19) with experimental data which were measured by Botello, Feliu and Climent on hydrogen adsorption at Pt(111) in 0.05 M NaOH [16],

$$H_2O + (1+\gamma)\,e + {}^* \leftrightarrow H_{ad}^{-\gamma} + OH^-. \tag{27}$$

with $\gamma < 0$, corresponding to a positively charged $H_{ad}^{-\gamma}$.

Different from the oxidative anion adsorption in equation (5), hydrogen adsorption in equation (27) is a reduction reaction. The reaction rate, positive-defined for the

Table 1. List of model parameters.

Symbol	Meaning	Value	Note
c_0	Bulk concentration	0.05 mol L^{-1}	Exp. condition in reference [16]
pH	Solution pH	12.7	Exp. condition in reference [16]
ϵ	Dielectric constant of bulk solution	78.5	Constant
l	Nernst diffusion layer thickness	100 μm	Common value
D	Diffusion coefficient	5.3×10^{-9} m^2 s^{-1}	Reference [56]
N_{site}	Adsorption site density	1.5×10^{19} m^{-2}	$4/\sqrt{3}a_{Pt}^{-2}$ with a_{Pt} being the lattice constant
ϕ_{pzc}	Potential of zero charge	0.28 V_{SHE}	Reference [57]
δ	Thickness of the space between the electrode and the AP	0.2 nm	Fitted, in reasonable range
ϵ'	Dielectric constant of the space between the electrode and the AP	2.5	Fitted, in reasonable range [55]
α	Effective charge transfer coefficient	0.45	Fitted, in reasonable range [58]
γ	Charge number on H_{ad}	−0.04	Fitted, close to DFT calculations [54]
E_0	Standard equilibrium potential of the reaction	0.28 V_{SHE}	Reference [43]
ξ	Lateral interaction coefficient	29.2 kJ mol^{-1}	Reference [43]
k_0	Rate constant	2.14×10^{-4} $\exp(-\frac{3.02\times10^4}{R}(\frac{1}{T}-\frac{1}{298.15}))$ mol m^{-2} s^{-1}	Fitted, the activation barrier is close to the value in reference [16]

oxidation direction, is now expressed as

$$J_{ad} = k_0 \left[C_{-,AP}\theta \exp\left(\frac{\alpha F\eta}{RT}\right) - (1-\theta)\exp\left(-\frac{(1-\alpha)F\eta}{RT}\right)\right], \quad (28)$$

with $\eta = (1+\gamma)(\phi_M - \phi_{AP}) - E_0 + \frac{\xi}{F}\theta$. Therefore, equation (8) determining θ_s is modified to

$$\frac{RT}{F}\ln\left(\frac{\theta_s}{1-\theta_s}\right) + (1-\gamma)\phi_M + \gamma\phi_{AP,s} + \frac{\xi}{F}\theta_s - E_0 = 0, \quad (29)$$

and the dimensionless adsorption resistance is changed to

$$R_{ad}^{nd} = \frac{2Dc_0}{k_0(1-\theta_s)\lambda_D} e^{(1-\alpha)H_s}. \quad (30)$$

Nevertheless, the impedance formula in equation (19) and its two coefficients Δ_1 and Δ_2 remain unaltered. When fitting experimental data at a range of electrode potentials, we need to replace C_{GC}^0 limited to the pzc, which appears in the reference impedance $\frac{2\lambda_D^2}{C_{GC}^0 D}$ and the capacitance ratio r_c, with [13, 53]

$$C_{GC} = C_{GC}^0 \frac{\cosh\left(\frac{\Delta U}{2}\right)}{1+2\gamma_c\sinh^2\left(\frac{\Delta U}{2}\right)}\sqrt{\frac{2\gamma_c\sinh^2\left(\frac{\Delta U}{2}\right)}{\ln\left(1+2\gamma_c\sinh^2\left(\frac{\Delta U}{2}\right)\right)}}, \quad (31)$$

which is applicable to any potential in the context of the PNP theory modified by considering the finite ion size effect, with $\Delta U = F\left(\phi_M - \phi_{pzc}\right)/RT$, $\gamma_c = c_0 N_A (d_c)^3$ the volume fraction of counterions (solvated Na^+ in our case) in the solution bulk, and d_c the length of the cube of the hydrated Na^+. The finite ion size effect considered in equation (31) can remedy the well-known Gouy–Chapman catastrophe, namely unphysically large C_{GC} at potentials far away from the pzc.

Figure 2 shows the comparison between the theory (lines) and experimental data (circles) at three temperatures (5, 25, 45 °C) and six potentials (0.05 V_{RHE} to 0.30 V_{RHE} in a step of 0.05 V). In the literature work, each EIS curve was fitted separately using the Frumkin–Melik–Gaikazyan model [16]. On the contrary, our model fitting is conducted all at once using the same set of parameters listed in table 1. In this manner, the degree of freedom of using different model parameters at varying temperatures and potentials is eliminated. The temperature and potential dependence of the impedance response are described consistently by physical theories used to build the model. As we have less freedom in the model fitting, the agreement between the model and the experiment is worse. Yet, we believe more important than the fitting agreement is the physical consistency.

Our theoretical formula captures essential features of experimental data, namely, a semicircle in the high frequency range and a capacitive line in the low frequency range. It is noteworthy that the well-known signature of the Warburg impedance, namely a 45° line, is missing, which will be explained at a

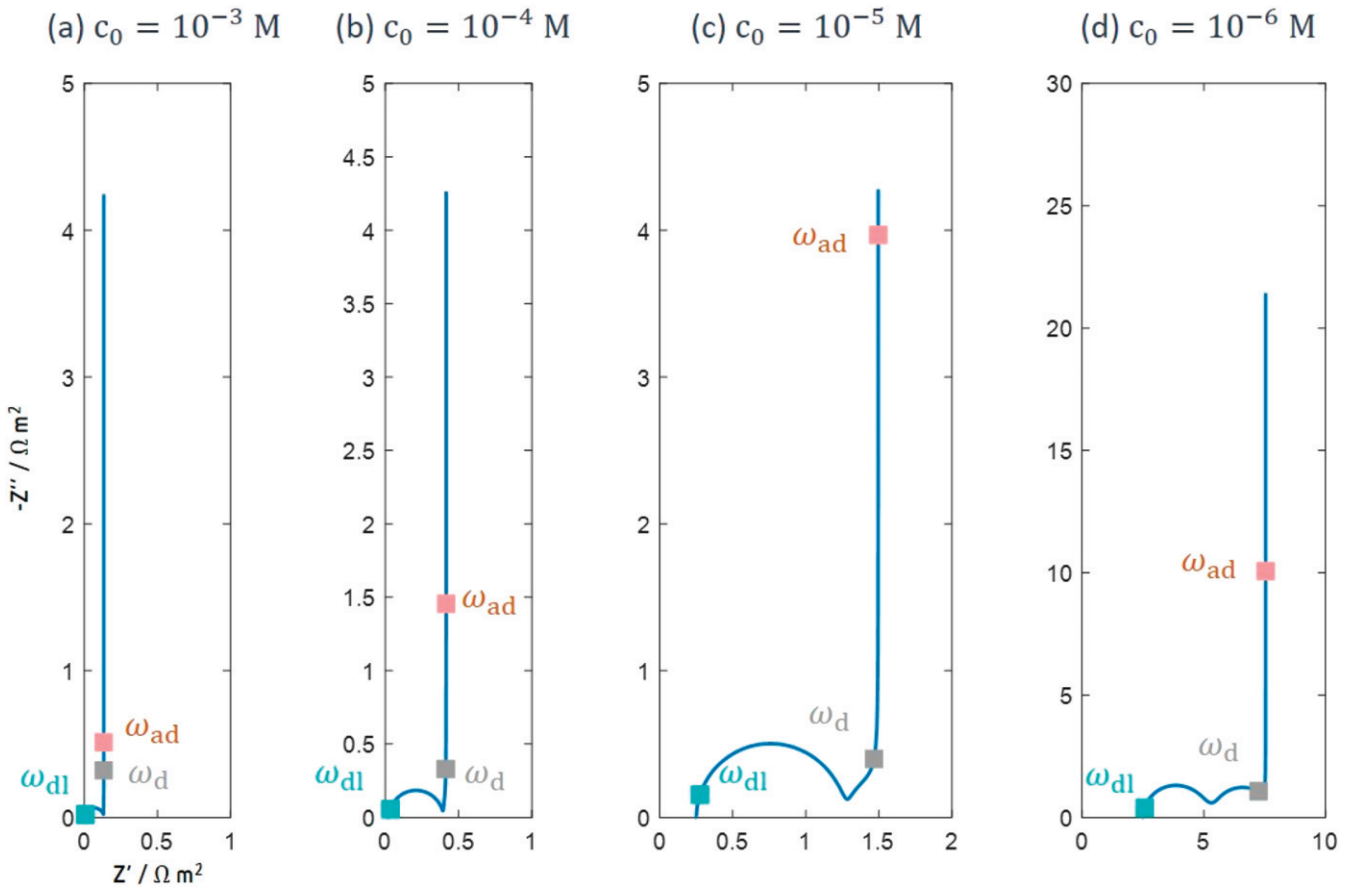

Figure 3. EIS of hydrogen adsorption at Pt(111) in x M NaOH at 0.15 V_{RHE} at room temperature. The concentration of NaOH is varied as follows: (a) 1 mM, (b) 0.1 mM, (c) 0.01 mM, and (d) 1 μM. Model parameters are listed in table 1. The frequency range is 10^6–10^{-2} Hz with ten points per decade in (a)–(c) and 10^6–10^{-3} Hz in (d).

later stage. Generally, the size of the semicircle grows at higher potentials, which is the consequence of more positive values of η according to equation (30), and at lower temperatures, which is the consequence of a lower k_0 with an activation energy of 30.2 kJ mol^{-1} (cf 32 kJ mol^{-1} in reference [16]). The remaining electron number on H_{ad} is -0.04, which is close to the value obtained from DFT calculations conducted at Pt(111) [54]. Nevertheless, we shall have in our mind that the remaining electron number is difficult to obtain accurately and depends on the theoretical method used, e.g. figure 7 in reference [40]. The parameters of the space between the electrode and the AP also fall into reasonable ranges [55]. The deviation between experiment and theory varies at different potentials, and it can be quite noticeable at some potentials. The main reason is ascribed to the inadequacy of the presented description of potential-dependent EDL structure and chemisorption kinetics.

5. Characteristic frequencies

Analyzing the characteristic frequencies of different processes is an integral part of grasping the EIS. To make life easier, we consider the ideal case of one-electron transfer reaction ($\gamma = 0$). Nonzero values of γ complicate the expressions, but do not change physical insights. Under the well-justified approximation of $L \gg 1$ and in the usual frequency range of $\omega^{nd} \ll 1$, the general formula in equation (19) is simplified to

$$Z^{nd} = R_s^{nd} + \frac{1}{2}\frac{1}{j\omega^{nd}C_{dl}^{nd}\left(1 + \frac{j\omega^{nd}C_{ad}^{nd}}{1+j\omega^{nd}R_{ad}^{nd}C_{ad}^{nd}}\frac{\tanh\left(L\sqrt{j\omega^{nd}}\right)}{\sqrt{j\omega^{nd}}}\right) + \frac{j\omega^{nd}C_{ad}^{nd}}{1+j\omega^{nd}R_{ad}^{nd}C_{ad}^{nd}}}, \tag{32}$$

where R_s^{nd} is given in equation (20). Three characteristic frequencies can be identified

$$\omega_{dl}^{nd} = \frac{1}{C_{dl}^{nd}R_{ad}^{nd}}, \qquad \omega_{ad}^{nd} = \frac{1}{C_{ad}^{nd}R_{ad}^{nd}}, \qquad \omega_{d}^{nd} = \frac{1}{L^2}, \tag{33}$$

corresponding to the EDL charging process, the chemisorption process, and the ion transport in the Nernst diffusion layer, respectively. ω_i^{nd} can be transformed to dimensional quantities using $\omega_i = \omega_i^{nd}D/\lambda_D^2$. In most cases, we have $C_{dl}^{nd} \ll C_{ad}^{nd}$, thus, $\omega_{dl}^{nd} \gg \omega_{ad}^{nd}$. However, the relation between ω_{ad}^{nd} and ω_d^{nd} is uncertain and subject to change by tuning experimental conditions.

Let us first examine the case of $\omega_{ad}^{nd} > \omega_d^{nd}$. Three types of impedance behaviors are obtained in different frequency ranges. In the high frequency range of $\omega^{nd} \gg \omega_{dl}^{nd}$, we have $Z^{nd} = R_s^{nd}$ as given in equation (20). At frequencies around ω_{dl}^{nd}, namely $\omega^{nd} \approx \omega_{dl}^{nd} \gg \omega_{ad}^{nd} > \omega_d^{nd}$, equation (32) is simplified to

$$Z^{\rm nd} = R_{\rm s}^{\rm nd} + \frac{1}{2}\frac{R_{\rm ad}^{\rm nd}}{j\omega^{\rm nd}C_{\rm dl}^{\rm nd}R_{\rm ad}^{\rm nd}+1}, \tag{34}$$

which corresponds to the high-frequency semicircle, with a width of $R_{\rm ad}^{\rm nd}$ and a characteristic frequency of $\omega_{\rm dl}^{\rm nd}$, in the EIS plot in figure 2. In the low frequency range of $\omega^{\rm nd} \ll \omega_{\rm ad}^{\rm nd}$, equation (32) is simplified to

$$Z^{\rm nd} = R_{\rm s}^{\rm nd} + \frac{1}{2}\frac{1}{j\omega^{\rm nd}\left(C_{\rm dl}^{\rm nd}+C_{\rm ad}^{\rm nd}\right)+O\left(j\omega^{\rm nd}\right)}, \tag{35}$$

which corresponds to the low-frequency capacitive line in the EIS plot in figure 2. $O\left(j\omega^{\rm nd}\right)$ means that the remaining part is less than the order of $j\omega^{\rm nd}$. Note that the salient feature of the Warburg diffusion impedance, namely a 45° line in the low frequency region, is absent in this case, which has not been explained before [16, 19, 20].

Let us then examine the other case of $\omega_{\rm ad}^{\rm nd} < \omega_{\rm d}^{\rm nd}$. The impedance behaviors in the frequency range of $\omega^{\rm nd} \gg \omega_{\rm dl}^{\rm nd}$ and $\omega^{\rm nd} \approx \omega_{\rm dl}^{\rm nd} \gg \omega_{\rm d}^{\rm nd} > \omega_{\rm ad}^{\rm nd}$ are the same as in the previous case. In the frequency range of $\omega_{\rm dl}^{\rm nd} \gg \omega^{\rm nd} \gg \omega_{\rm d}^{\rm nd} > \omega_{\rm ad}^{\rm nd}$, we obtain

$$Z^{\rm nd} = R_{\rm s}^{\rm nd} + \frac{1}{2}\frac{R_{\rm ad}^{\rm nd}}{1+C_{\rm dl}^{\rm nd}\sqrt{j\omega^{\rm nd}}}, \tag{36}$$

implying a 45° line in the Nyquist plot. At even lower frequencies, equation (35) is re-obtained.

The above analysis explains the absence of diffusion signature in the chemisorption impedance in figure 2. It is simply because the experimental condition falls into the regime of $\omega_{\rm ad}^{\rm nd} > \omega_{\rm d}^{\rm nd}$. One can lower the bulk concentration c_0 in order to observe the 45° line in the low frequency region, see figure 3. We note that measuring EIS at very low concentration, say <10 mM, is a frontier challenge for experimentation.

As for the ion transport process, $\omega_{\rm d} = D/l^2$ is independent of c_0. As for the adsorption process, substitution of $R_{\rm ad}^{\rm nd}$ and $C_{\rm ad}^{\rm nd}$ into equation (33) leads to $\omega_{\rm ad} \propto {\rm e}^{\frac{(1-\alpha)F\phi_{\rm AP}}{RT}}$. When the electrode potential is fixed and when the electrode is negatively charged, which is the case for Pt(111) in alkaline solutions in the potential range of hydrogen adsorption, $\phi_{\rm AP}$ becomes more negative at lower c_0s. Therefore, $\omega_{\rm ad}$ will decrease at lower c_0s. In figures 3(a)–(d), $\omega_{\rm ad}$ approaches $\omega_{\rm d}$ to a greater extent as increasing c_0. Consequently, the diffusion signature tends to disappear. It is interesting to note that the concentration dependence of $\omega_{\rm ad}$ is a manifestation of the surface charge effects (Frumkin corrections [5, 36]). In addition, the diffusion impedance manifests as a semicircle in figure 3(d). This is a salient feature of the bounded diffusion, which cannot be described by the Warburg formula [27].

6. Conclusion

In conclusion, an analytical formula of chemisorption impedance, exact at the pzc, has been derived from the one-dimensional PNP theory for the ion transport process in the solution region coupled with the Frumkin–Butler–Volmer theory for the partial electron transfer at the electrode surface. The chemisorption-induced surface dipole moment is considered. Characteristic frequencies and asymptotic behaviors of the obtained formula are obtained in analytical forms. The classical Frumkin–Melik–Gaikazyan model is retrieved with three additional clearly-defined assumptions. The absence of the signature of the Warburg impedance in experimental data is explained. It is important to note that the analytical formula is valid only for a dilute solution made of monovalent ions with equal diffusivity in the presence of a weakly charged electrode surface. One may have to resort to numerical solutions in more general situations. However, we hope the readers can agree on the value of analytical models in obtaining physical insights that are instrumental to a wide range of conditions and systems.

Associated content

In the supporting information, we provide a detailed derivation of the chemisorption impedance, and changes made for the case of cation specific adsorption.

Conflict of interest

The authors declare no competing financial interests.

Acknowledgments

This work is financially supported by the Alexander von Humboldt Foundation, and National Natural Science Foundation of China under the Grant number of 21802170. The authors are grateful to Prof. Victor Climent for sharing the original experimental data and to Prof. Tamas Pajkossy for helpful discussion.

Data availability statement

The data generated and/or analysed during the current study are not publicly available for legal/ethical reasons but are available from the corresponding author on reasonable request.

ORCID iDs

Jun Huang https://orcid.org/0000-0002-1668-5361

References

[1] Muscat J P and Newns D M 1978 Chemisorption on metals *Prog. Surf. Sci.* **9** 1–43
[2] Hammer B and Nørskov J K 2000 *Advances in Catalysis* (New York: Academic) pp 71–129
[3] Schmickler W 2017 *Electrochemical Science for a Sustainable Society: A Tribute to John O'M Bockris* ed K Uosaki (Basel: Springer) pp 95–111
[4] Grahame D C 1947 The electrical double layer and the theory of electrocapillarity *Chem. Rev.* **41** 441–501
[5] Frumkin A N 1960 The double layer in electrochemistry *J. Electrochem. Soc.* **107** 461

[6] Schmickler W and Guidelli R 2014 The partial charge transfer *Electrochim. Acta* **127** 489–505

[7] Attard G A 2018 A phenomenological theory of electrosorption *J. Electroanal. Chem.* **819** 481–94

[8] Huang J and Chen S 2018 Interplay between covalent and non-covalent interactions in electrocatalysis *J. Phys. Chem.* C **122** 26910–21

[9] Huang J, Li P and Chen S 2019 Quantitative understanding of the sluggish kinetics of hydrogen reactions in alkaline media based on a microscopic Hamiltonian model for the Volmer step *J. Phys. Chem.* C **123** 17325–34

[10] Pacchioni G and Bagus P S 1989 Point-charge effects on the vibrational frequency of CO chemisorbed on Cu and Pd clusters: a model for CO with ionic coadsorbates *Phys. Rev.* B **40** 6003–11

[11] Climent V, García-Araez N and Feliu J M 2006 Influence of alkali cations on the infrared spectra of adsorbed (bi)sulphate on Pt(111) electrodes *Electrochem. Commun.* **8** 1577–82

[12] Huang J, Malek A, Zhang J and Eikerling M H 2016 Non-monotonic surface charging behavior of platinum: a paradigm change *J. Phys. Chem.* C **120** 13587–95

[13] Huang J, Zhou T, Zhang J and Eikerling M 2018 Double layer of platinum electrodes: non-monotonic surface charging phenomena and negative double layer capacitance *J. Chem. Phys.* **148** 044704

[14] Martínez-Hincapié R, Climent V and Feliu J M 2018 Peroxodisulfate reduction as a probe to interfacial charge *Electrochem. Commun.* **88** 43–6

[15] Sibert E, Faure R and Durand R 2001 High frequency impedance measurements on Pt(111) in sulphuric and perchloric acids *J. Electroanal. Chem.* **515** 71–81

[16] Botello L E, Feliu J M and Climent V 2020 Activation energy of hydrogen adsorption on Pt(111) in alkaline media: an impedance spectroscopy study at variable temperatures *ACS Appl. Mater. Interfaces* **12** 42911–7

[17] Dolin P and Ershler B 1940 The kinetics of discharge and ionization of hydrogen adsorbed at Pt-electrode *Acta Physicochim. URSS* **13** 747

[18] Ershler B 1947 Investigation of electrode reactions by the method of charging-curves and with the aid of alternating currents *Discuss. Faraday Soc.* **1** 269–77

[19] Kerner Z and Pajkossy T 2002 Measurement of adsorption rates of anions on Au(111) electrodes by impedance spectroscopy *Electrochim. Acta* **47** 2055–63

[20] Pajkossy T and Kolb D M 2001 Double layer capacitance of Pt(111) single crystal electrodes *Electrochim. Acta* **46** 3063–71

[21] Sluyters-Rehbach M J P 1994 Impedances of electrochemical systems: terminology, nomenclature and representation-part I: cells with metal electrodes and liquid solutions (IUPAC recommendations 1994) *Pure Appl. Chem.* **66** 1831–91

[22] Huang J 2020 Electrochemical impedance spectroscopy for electrocatalytic interfaces and reactions: classics never die *J. Electrochem.* **26** 3–18

[23] Warburg E 1899 Ueber das Verhalten sogenannter unpolarisirbarer Elektroden gegen Wechselstrom *Ann. Phys., Lpz.* **303** 493–9

[24] Li C K and Huang J 2021 Impedance response of electrochemical interfaces: part I. Exact analytical expressions for ideally polarizable electrodes *J. Electrochem. Soc.* **167** 166517

[25] Walters M J, Garland J E, Pettit C M, Zimmerman D S, Marr D R and Roy D 2001 Weak adsorption of anions on gold: measurement of partial charge transfer using Fast Fourier Transform electrochemical impedance spectroscopy *J. Electroanal. Chem.* **499** 48–60

[26] Robertson W D 1953 The capacity of polarized platinum electrodes in hydrochloric acid *J. Electrochem. Soc.* **100** 194–201

[27] Huang J 2018 Diffusion impedance of electroactive materials, electrolytic solutions and porous electrodes: Warburg impedance and beyond *Electrochim. Acta* **281** 170–88

[28] Huang J, Li Z, Ge H and Zhang J 2015 Analytical solution to the impedance of electrode/electrolyte interface in lithium-ion batteries *J. Electrochem. Soc.* **162** A7037–48

[29] Huang J, Ge H, Li Z and Zhang J 2014 An agglomerate model for the impedance of secondary particle in lithium-ion battery electrode *J. Electrochem. Soc.* **161** E3202–15

[30] Huang J, Li Z, Zhang J, Song S, Lou Z and Wu N 2015 An analytical three-scale impedance model for porous electrode with agglomerates in lithium-ion batteries *J. Electrochem. Soc.* **162** A585–95

[31] Huang J and Zhang J 2016 Theory of impedance response of porous electrodes: simplifications, inhomogeneities, non-stationarities and applications *J. Electrochem. Soc.* **163** A1983–2000

[32] Huang J, Gao Y, Luo J, Wang S, Li C, Chen S and Zhang J 2020 Editors' choice-review-impedance response of porous electrodes: theoretical framework, physical models and applications *J. Electrochem. Soc.* **167** 166503

[33] Sun Y, Eikerling M, Zhang J and Huang J 2020 Impedance model of a water-filled Pt nanopore: interfacial charging and chemisorption effects *J. Electrochem. Soc.* **167** 066519

[34] Kornyshev A A and Schmickler W 1986 On the coverage dependence of the partial charge transfer coefficient *J. Electroanal. Chem. Interfacial Electrochem.* **202** 1–21

[35] Huang J 2020 Mixed quantum-classical treatment of electron transfer at electrocatalytic interfaces: theoretical framework and conceptual analysis *J. Chem. Phys.* **153** 164707

[36] Frumkin A 1933 Wasserstoffüberspannung und Struktur der Doppelschicht *Z. Phys. Chem.* **164A** 121–33

[37] Dickinson E J F and Wain A J 2020 The Butler–Volmer equation in electrochemical theory: origins, value, and practical application *J. Electroanal. Chem.* **872** 114145

[38] Dreyer W, Guhlke C and Müller R 2013 Overcoming the shortcomings of the Nernst–Planck model *Phys. Chem. Chem. Phys.* **15** 7075–86

[39] Gillespie D 2015 A review of steric interactions of ions: why some theories succeed and others fail to account for ion size *Microfluid. Nanofluid.* **18** 717–38

[40] Ávila M, Juárez M F and Santos E 2020 Role of the partial charge transfer on the chloride adlayers on Au(100) *ChemElectroChem* **7** 4269–82

[41] van Soestbergen M 2012 Frumkin-Butler-Volmer theory and mass transfer in electrochemical cells *Russ. J. Electrochem.* **48** 570–9

[42] Climent V, Gómez R, Orts J M and Feliu J M 2006 Thermodynamic analysis of the temperature dependence of OH adsorption on Pt(111) and Pt(100) electrodes in acidic media in the absence of specific anion adsorption *J. Phys. Chem.* B **110** 11344–51

[43] Garcia-Araez N, Climent V and Feliu J M 2010 Analysis of temperature effects on hydrogen and OH adsorption on Pt(111), Pt(100) and Pt(110) by means of Gibbs thermodynamics *J. Electroanal. Chem.* **649** 69–82

[44] Macdonald J R 2011 Effects of various boundary conditions on the response of Poisson–Nernst–Planck impedance spectroscopy analysis models and comparison with a continuous-time random-walk model *J. Phys. Chem.* A **115** 13370–80

[45] Macdonald J R and Franceschetti D R 1978 Theory of small-signal ac response of solids and liquids with recombining mobile charge *J. Chem. Phys.* **68** 1614–37

[46] Lelidis I and Barbero G 2005 Effect of different anionic and cationic mobilities on the impedance spectroscopy measurements *Phys. Lett.* A **343** 440–5

[47] Lelidis I, Ross Macdonald J and Barbero G 2015 Poisson–Nernst–Planck model with Chang–Jaffe, diffusion, and ohmic boundary conditions *J. Phys. D: Appl. Phys.* **49** 025503

[48] Duarte A R, Batalioto F, Barbero G and Neto A M F 2013 Electric impedance of a sample of dielectric liquid containing two groups of ions limited by ohmic electrodes: a study with pure water *J. Phys. Chem.* B **117** 2985–91

[49] Lenzi E K, Evangelista L R, Taghizadeh L, Pasterk D, Zola R S, Sandev T, Heitzinger C and Petreska I 2019 Reliability of Poisson–Nernst–Planck anomalous models for impedance spectroscopy *J. Phys. Chem.* B **123** 7885–92

[50] Moškon J, Žuntar J, Drvarič Talian S, Dominko R and Gaberšček M 2020 A powerful transmission line model for analysis of impedance of insertion battery cells: a case study on the NMC-Li system *J. Electrochem. Soc.* **167** 140539

[51] Moškon J and Gaberšček M 2021 Transmission line models for evaluation of impedance response of insertion battery electrodes and cells *J. Power Sources Adv.* **7** 100047

[52] Frumkin A N and Petrii O A 1975 Potentials of zero total and zero free charge of platinum group metals *Electrochim. Acta* **20** 347–59

[53] Kornyshev A A 2007 Double-layer in ionic liquids: paradigm change? *J. Phys. Chem.* B **111** 5545–57

[54] Bonnet N and Marzari N 2013 First-principles prediction of the equilibrium shape of nanoparticles under realistic electrochemical conditions *Phys. Rev. Lett.* **110** 086104

[55] Bockris J O M, Devanathan M A V and Müller K 1963 On the structure of charged interfaces *Proc. R. Soc.* A **274** 55–79

[56] Light T S, Licht S, Bevilacqua A C and Morash K R 2005 The fundamental conductivity and resistivity of water *Electrochem. Solid-State Lett.* **8** E16

[57] Rizo R, Sitta E, Herrero E, Climent V and Feliu J M 2015 Towards the understanding of the interfacial pH scale at Pt(111) electrodes *Electrochim. Acta* **162** 138–45

[58] Rolando G, Richard G C, Juan M F, Eliezer G, Jacek L, Wolfgang S and Sergio T 2014 Defining the transfer coefficient in electrochemistry: an assessment (IUPAC technical report) *Pure Appl. Chem.* **86** 245–58